BBAA VI International Colloquium on:
Bluff Bodies Aerodynamics & Applications
Milano, Italy, July, 20-24 2008

CALCULATION OF THE CROSSWIND DISPLACEMENT OF PANTOGRAPHS

Abdessalem Bouferrouk[*], Chris J Baker[*] , Mark Sterling[*] H O'Neil[+] and S Wood[+]

[*]School of Civil Engineering
The University of Birmingham, Edgbaston, Birmingham, B15 2TT, UK
e-mail:A.Bouferrouk@bham.ac.uk
[+] Interfleet Technology Ltd, Interfleet House, Pride Parkway, Debry, DE24 8HX, UK

Keywords: Crosswind, Aerodynamic Admittance, Weighting Function, Pantograph, Contact Wire

Abstract *The static crosswind displacements of a high speed pantograph and contact wire are studied. The aim is to assess the overall pantograph sway in crosswinds based on the relative movements of the pantograph and contact wire, taking into account the crosswind deflection of the train body. The pantograph and wire deflections are derived from simplified models of such structures, whereas train body displacements are computed via Vampire. A spectral approach is used to simulate the turbulent crosswind, which is then used with aerodynamic admittance function to obtain unsteady crosswind loading. Analysis of data shows negligible crosswind deflections of the pantograph itself in the range of few millimeters, but train body and wire deflections are much larger. It is shown that crosswinds may cause the pantograph sway to exceed prescribed limits for some combinations of wind gust and track conditions.*

1 INTRODUCTION

The issue of high speed train reaction to crosswinds has been the subject of many research studies, both experimental and computational. This project is a summary of current work being undertaken at the University of Birmingham, UK, which encompasses the two studies by Baker et al. [1] and Sterling et al. [2]. It is a sponsored project that was carried out in collaboration with Interfleet Technology, Derby, UK, to investigate the sway of train pantographs in high crosswinds, to ensure the displacement of pantograph relative to the contact wire is kept within acceptable limits. As will be seen, the study consists of undertaking wind tunnel tests of a scaled model of a high speed train in crosswinds. The experimental data will be used to develop analytical formulations for predicting pantograph and contact wire deflections in high crosswinds. Interfleet Technology were then able to input these deflections in a dynamic model of the UK Class 365 EMU train to determine the overall pantograph sway for a wide range of crosswind and train speeds.

Increasing the speed and decreasing the weight of high speed trains have led to increased sensitivity to crosswind effects [3]. In particular, calculation of the overturning risk of trains has received considerable interest; see for example [4] and [5]. To complement such work, this study investigates in addition to train displacement, the pantograph and contact wire static

movements under crosswinds. Knowledge of pantograph and wire deflections is important in train operations because if such displacements are appreciable enough, they may cause contact loss between the pantograph and contact wire, leading to loss of electrical power supply (or dewirement). The important aerodynamic forces affecting the train body, its pantograph, and the contact wire in crosswinds consist of lift and side force components. In this work, only the effects of side force are considered. Some previous research has looked into the crosswind interaction with the catenary and contact wire, e.g. [6], while currently there is a European interest regarding the combined effects of crosswinds both on the catenary and pantograph [7]. The present study investigates the impact of crosswinds on a high speed pantograph by considering both the mean flow and the turbulence effects.

2 OUTLINE OF THE METHOD

The procedure to compute the deflections and thus the pantograph sway consists of the following steps

1) The generation of a turbulent crosswind velocity time history
2) Wind tunnel tests of a scaled model of the Class 365 EMU to compute the mean force coefficients for a number of relative wind angles
3) In the frequency domain, aerodynamic admittance functions for lift and side force are obtained on the basis of wind and force spectra
4) Expressions for the aerodynamic admittance function are derived. Corresponding expressions of the aerodynamic weighting function are obtained in the time-domain
5) By convolving the weighting function with crosswind velocity the fluctuating part of the crosswind force on the train is found, which is added to the mean force to obtain the total unsteady force on the train.
6) These forces are then used to calculate the deflections of the train body due to crosswinds for a range of variables – wind speed, vehicle speed, track roughness, cant etc, using the dynamic analysis software Vampire
7) Suitable models of pantograph and contact wire deflections due to crosswind are derived
8) The deflections from (7) are then used with the predictions of Vampire to compute total pan sway values in crosswinds.

3 COMPONENTS OF THE METHOD

3.1 Crosswind time history simulation

Let us consider the UK Class 365 EMU train fitted with a pantograph, running on an electrified straight track through a turbulent crosswind which acts perpendicular to the train (pure crosswind). The crosswind flow is two-dimensional, incompressible, and has a mean and a fluctuating (turbulent) part which needs to be simulated. The turbulent crosswind impinges on the train body and the pantograph/overhead wire system, creating a fluctuating side force. In order to account for this unsteady loading, the time history of the turbulent velocity input must be properly simulated. Turbulent velocity is a random process with correlated time and length scales. On the premise that the spectral approach has been successful in modeling random stochastic processes in addition to ease of implementation, it is used here to generate a multiple-point correlated crosswind velocity field along the track. Only the longitudinal turbulent component $u'(t)$ will be simulated. The turbulent velocity is based on Kaimal's spectrum [8] of wind frequencies, and incorporates a Davenport's spatial coherence function at a height $z = 3\ m$ above the ground. Full details of the method can be

found in Ding et al. [9]. Fig. (1) is a time slice of a simulated longitudinal turbulent velocity with zero mean.

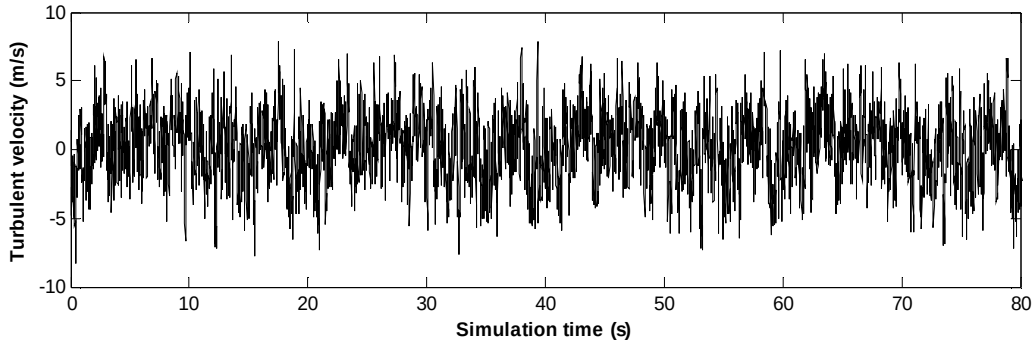

Figure 1: Sample time series of simulated longitudinal turbulent velocity

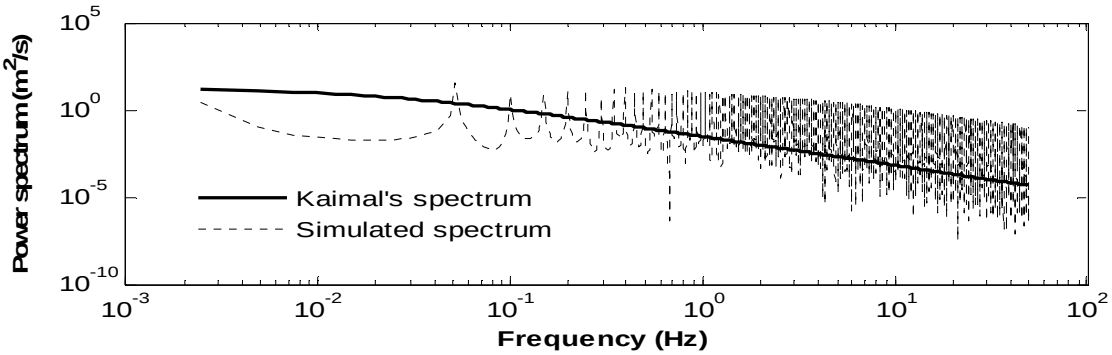

Figure 2: Comparison of simulated wind spectrum with Kaimal's true spectrum (log-log scale)

In Fig. (2), the power spectral density function of the simulated velocity is compared with Kaimal's true spectrum (using a log-log scale). Generally, there is a good agreement between the two spectra, indicating that velocity turbulent characteristics are fairly well reproduced. One should notice, however, that while the Kaimal's spectrum is heavily filtered, the current data contains high levels of noise as seen from the large fluctuations in the power spectra. From Fig. (2), the spectrum of turbulent velocity fluctuations has a slope of about -5/3 in accordance with Kolmogorov's power law of energy spectrum in the "inertial range" of turbulence, separating the scale at which energy is injected into large eddies from the much smaller scale at which viscous dissipation occurs.

3.2 Aerodynamic force time history simulation

Once the turbulent crosswind has been simulated, the next step is to calculate the resulting unsteady forces on the train, the pantograph, and the contact wire. Different force calculation methods exist, including the traditional quasi-steady approach in which the force fluctuations follow wind perturbations without any lag or attenuation. This means only the fluctuations due to the instantaneous turbulence are captured while the unsteady memory effects of preceding turbulent velocities are ignored. Despite being straightforward to apply, the quasi-steady theory is known to produce large errors. For a crosswind flow which develops over a large surface of a moving train a method is needed to account for both train movement and flow development in the vicinity of the train surface. These issues are addressed here using the concept of aerodynamic admittance function. As will be shown later, however, use of admittance functions is not required for the pantograph and contact wire since they react to

different turbulent length scales compared with the main body. The idea of aerodynamic admittance was extended from the aeronautical field to wind engineering by Davenport [10]. Calculations involving aerodynamic admittance function are usually carried out in the frequency domain, but the need to compute unsteady forces means a time-domain procedure is required. This is achieved via the so-called aerodynamic weighting function.

As discussed in Baker et al. [1], a 1:30th scale model of the Class 365 EMU was commissioned for wind tunnel testing at RWDI Anemos site, UK. Fig. (3) shows the model in a wind tunnel static test. The vehicle model consists of 4 cars, the second car has a pantograph fitted on top of it and the measured forces on its surface were used as inputs in Vampire to estimate car body movement in crosswinds. The loadings on the leading car were intended for use in a separate study on train overturning in crosswinds. Further details of this work are found in [11]. The magnitude of the aerodynamic loading depends on the relative wind speed U_R between the wind direction and train direction of travel so that $U_R = \sqrt{V^2 + u^2(t)}$, with V being the vehicle speed and U the mean wind speed. The relative direction between the train and the wind is called the yaw angle β. For a pure crosswind as in Fig. (4), the yaw angle is defined as $\beta = \tan^{-1}(V/u(t))$, where $u(t)$ is the absolute wind velocity ($u(t) = U + u'(t)$).

Figure 3: A 1:30th scale model of a 4-car Class 365 EMU in the RWDI-Anemos wind tunnel

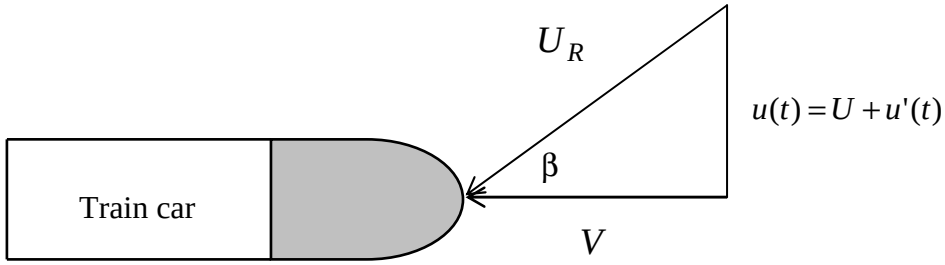

Figure 4: Definition of yaw angle and relative wind velocity for a pure crosswind

The flow past the train was measured for six yaw angles (15, 30, 45, 60, 75, and 90°) at varying magnitudes of wind speed. In each case, the pressure tapping measurements around the car surface allowed the calculation of time-averaged (mean) crosswind forces (lift and side force). These forces were then non-dimensionalised in the usual manner to obtain the corresponding mean aerodynamic force coefficients as a function of yaw angle. Knowing how the mean force coefficients vary with yaw angle will enable us to determine the aerodynamic forces for any value of crosswind.

From the pressure measurements around the model train, force and moment spectra were then computed for the six yaw angles. These spectra enable the definition, in the frequency domain, of the aerodynamic admittance function as shown by Baker [5]

$$\left|X_F(n)\right|^2 = \frac{4S_F(n)}{(\rho AC_F)^2 U^2 S_U(n)} \qquad (1)$$

where $S_F(n)$ and $S_U(n)$ are, respectively, the power spectral densities of force and velocity, ρ is the density of air, A is a reference side area, C_F is the mean force coefficient, and n is the frequency. The admittance function has magnitude and phase shift $\phi_F(n)$ and it is effectively the ratio of the force power spectrum to the wind power spectrum. It represents a correction to the conventional quasi-steady theory often used in wind engineering. In the time-domain, the equivalent expression is called the weighting function which needs to be determined. While both $S_F(n)$ and $S_U(n)$ can be measured at full scale or model scale giving the admittances, the phase $\phi_F(n)$ is not easy to determine because wind velocities and forces are not usually measured sufficiently close together at the same time. The following approach to determine the weighting functions was thus adopted as in [5]. From the wind tunnel experiments, the lift and side force admittance functions were estimated. Typical admittance functions for side force as a function of β are illustrated in Fig. (5).

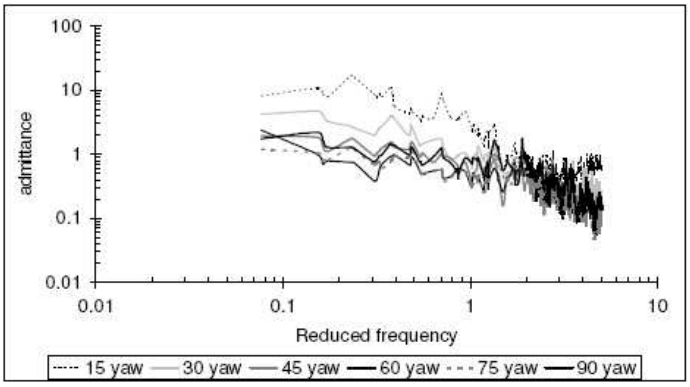

Figure 5: Side force aerodynamic admittance functions for a 1:30th scale model of the Class 365 EMU [1]

Using curve fits of data in Fig. (5), the admittance function may be parameterised as

$$\left|X_F(n)\right|^2 = \frac{1/k}{\left(1-\left(\frac{n}{n'}\right)^2\right)^2 + \left(2\zeta\frac{n}{n'}\right)^2} \qquad (2)$$

The parameters n', ξ, and k are constants and have no physical meaning. By making some assumptions concerning ζ and k as explained in [2], the time domain equivalent expression for admittance, i.e. the weighting function, may be shown to take the form

$$h_F(\tau) = \left(2\pi\bar{n}'\right)^2 \left(\frac{U_R}{L}\right)^2 \tau \left[\exp^{\left(-2\pi\bar{n}'\frac{U_R}{L}\right)\tau}\right] \qquad (3)$$

where $\bar{n}' = n'\frac{L}{U}$, L is the vehicle's length (~ 20 *m*), and τ the weighting function time lag. The values of $\bar{n}'$ (either for lift or side force) were determined experimentally as a function of yaw angle based on the formulation in Eq. (2). The weighting functions are thus found from the measured admittance functions. The weighting function clearly depends on the relative wind, the vehicle length, and time lag. It has an exponentially decaying form, implying it becomes zero after some characteristic time period. As noted in [1], since the rolling moment is effectively the product of the side force and a moment arm about the c.g. (assumed constant), the aerodynamic admittance and weighting functions for the rolling moment will be similar to those for the side force.

Now that the weighting functions are computed, the unsteady forces are obtained through the weighting functions by adding the averaged and fluctuating parts,

$$F(t) = \bar{F} + F'(t) = 0.5\rho A C_F \bar{U}_R^2 + \rho A C_F \bar{U}_R \int_0^\infty h_F(\tau) u'(t-\tau) d\tau \qquad (4)$$

where F is either the side or lift force, and $h_F(\tau)$ is the aerodynamic weighting function of the force being considered. An overbar indicates a mean value, and a' represents the fluctuating part. It can thus be seen from Eq. (4) that the force time histories on a train can be determined from the velocity time histories if the appropriate force coefficients and weighting functions are known. The fluctuating part $F'(t)$ can be computed either in the time domain by expressing the integral as a convolution $h_F(\tau) * u'(t)$ (since the system is causal), or in the frequency domain by taking a Fourier transform for $F'(t)$, which transforms the integral to a product of the Fourier transforms of $h_F(\tau)$ and $u'(t)$, and then taking an inverse Fourier transform of the result. Sample results for side force history at U = 10 *m/s* and different trains speeds is shown in Fig. (6).

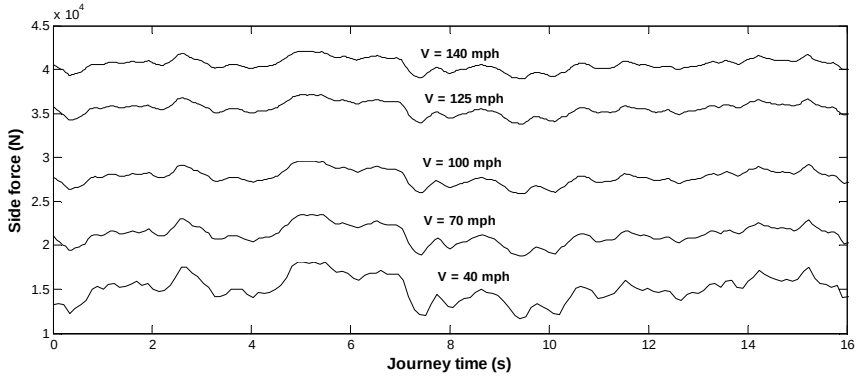

Figure 6: Side force histories on the Class 365 EMU at U = 10 *m/s* and different train speeds

The unsteady side force histories are used in Vampire as dynamic inputs into the stability analysis of the Class 365 model, taking into account other forces such as gravitational, and acceleration forces. Detailed information about the nature of unsteady crosswind forces on the

Class 365 EMU train can be found in [1], whereas reference [2] provides an investigation of the behaviour of the aerodynamic admittance functions for different train shapes.

The weighting functions represent the contribution of preceding turbulent crosswind velocities to the current value of unsteady aerodynamic force. In a discrete formulation in which the forces are computed at discrete locations along a track, the side force may be written as

$$F_S = 0.5\rho A C_S \overline{U}_R^2 + \rho A C_S \overline{U}_R \sum h_F(\tau) u'(t-\tau)\Delta\tau \qquad (5)$$

An interesting observation regarding Eq. (5) is that the effects of the weighting function, and thus the fluctuating force, become more pronounced if the integration time step $\Delta\tau$ is very small. The integration time step can be reduced by making the distance between the simulation points smaller, implying a larger number of simulation points. This is, however, computationally more expensive due to massive computing requirements to simulate a larger number of turbulent velocities through the spectral approach. Another important time scale is the characteristic time period of the weighting function τ_h after which the weighting function is zero. The weighting function may be regarded as a low pass filter which smoothes high frequency, short period fluctuations of periods less or equal than the characteristic time period τ_h, and diminishes any fluctuations for time periods where the weighting function falls to zero as time increases beyond $t = \tau_h$. The characteristic time step for the weighting function depends on the integration time step since in our case the time step in the integration of the weighting function is the same as the time step for force calculations.

3.3 Pantograph displacement calculations

For a high speed train, the overhead wire must maintain solid contact with the pantograph under all conditions in order to provide a stable supply of electrical current for the locomotive. This may be achieved through an active pantograph by maximising its ability to follow the catenary [12]. Mechanical, dynamic, and aerodynamic effects can strongly affect the supply of the contact force and particularly at high speeds loss of contact may occur. This part of the study investigates the influence of crosswinds on the static displacements of the pantograph and contact wire to assess whether such displacements are appreciable enough to cause contact loss between the pantograph and overhead wire. Specifically, the aim is to find out if such displacements are within permissible values as specified by UK standards.

The authors in [7], the authors investigated the effect of turbulence of the incoming flow due to train speed on the pantograph-catenary system to establish the wind dynamic effects on the contact force, but did not consider the effects of crosswinds. The present work investigates the effects on high speed trains of both the mean crosswind flow as well as the turbulence. The aerodynamic forces affecting the pantograph and contact wire in crosswinds consist of a lifting force, and a side force. Other forces such as the aerodynamic drag are mainly important for energy considerations. Although the wind tunnel data provides information on forces on the main vehicle, no forces were measured on the pantograph for two reasons. First, at 1:30th scale, the parts of the pantograph are very small and well into the size range where they would have been affected by Reynold number changes – i.e. transitions from sub- to super- critical flow separations etc, and thus modelling would have been difficult. Second, the forces on the pan in comparison to the main car are much smaller. Thus, some type of modeling is required. Typically, the pantograph of a UK high speed train consists of two registration arms and a pan head as depicted in Fig. (7). The two arms, a lower and an upper arm, are hinged together, the upper arm in turn being hinged to the pan head. The two rigid arms are cantilever beams

linked together such that the total deflection due to a uniform crosswind occurs at the top of the upper arm. This loading situation is depicted in Fig. (7). The way in which the two arms are hinged prevents any lateral twist so the arms can only deflect in the crosswind direction. The maximum deflection at point **B** can be shown to be

$$dB = \frac{wL_1^4}{8EI_1} + \frac{wL_1^3 L_2}{3EI_1} - \frac{wL_1^2 L_2^2}{4EI_1}\cos(\theta) \qquad (6)$$

so that the total deflection that occurs at point **C** is

$$dC = dB + \frac{wL_2^3 L_1}{2K_1 G}\sin(\theta) + \frac{wL_2^4}{8EI_2} \qquad (7)$$

Here, G is the shear modulus (GPa), E is Young's modulus, I the second moment of area, K_1 is a torsional constant, and w is the side force per unit length. Based on advice from the manufacturers of the Class 365 pantograph (Brecknell Willis, UK), the lower arm has a box cross-section with a typical wall thickness of 2 *mm*, while the upper arm is tubular with similar wall thickness. The hinge angle θ may change during a given journey. We consider a value of $\theta = 30^\circ$. The parameter K_1 corresponds to the upper arm and is defined as

$$K_1 = \frac{\pi}{2}\left(\frac{d}{2}\right)^4 \qquad (8)$$

d is the radius of the tubular upper arm, and G = 79 GPa for mild steel. A summary of the physical parameters of the arms is found in Table 1. The length scales to which the pan will react are of the order of pan height i.e. around 0.1 *m*. For a mean wind speed of U = 20 *m/s*, this gives a frequency of around 200 *Hz* where the energy content in the wind is very low. Thus, it is reasonable to consider the pan to react to the instantaneous speed, i.e. $U + u'(t)$. Therefore, the side force on each arm of the pan is obtained without consideration of past unsteady memory effects (i.e. quasi-steady), such that the weighting function integral $\int h_S(\tau)d\tau = 1$. However, if we are interested in studying the possible impact of crosswinds on suspension modes of above say 1-2 *Hz*, the weighting function method would have to be used. The unsteady side force is simply

$$F_{SP}(t) = 0.5\rho A\left(U + u'(t)\right)^2 C_S \qquad (9)$$

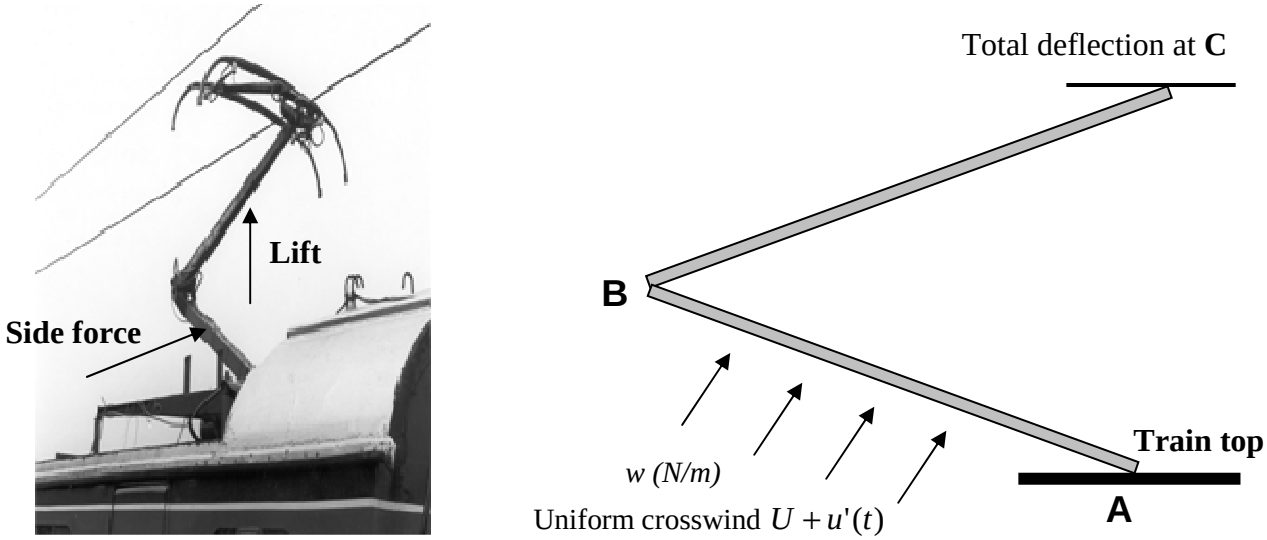

Figure 7: Crosswind forces on a high speed pantograph and their modelling

Independently of the train, the crosswind is assumed to act at right angles to the two arms with the side force in the along-wind direction viewed as a drag force. It is thus necessary to obtain approximate values of drag coefficients for aerodynamic shapes representative of a pan arm at $90°$ to the upstream flow.

Parameter	Lower arm (**AB**)	Upper arm (**BC**)
I (m^4)	7.5486×10^{-7}	7.3952×10^{-7}
E (N/m^2)	210×10^{9}	210×10^{9}
Length (*m*)	1.5	1.5
Cross-section	Box (wall thickness 2 *mm*)	Tubular (wall thickness 2 *mm*)

Table 1: Physical parameters used in calculating the pantograph deflection

The flow about each arm may be considered as that around a flat plate. For a mean crosswind of 20 *m/s* and a plate width of about 0.1 *m*, the Reynolds number (Re) is on the order of 10^5. The drag coefficient for a two-dimensional flat plate normal to a turbulent flow at this Re is $C_D = C_S$ = 1.2 [14]. For the upper tubular arm a slightly lower drag coefficient is used, C_D = 1.0 [14], since the drag coefficient for a rectangular cross section with sharp edges is likely to be higher than that for a circular section, due to stronger shed vortices. In addition to pan crosswind deflection, Brecknell Willis advises on additional 2 *mm* lateral movement of the pan head at full extension arising from radial play in the needle roller pivot bearings, with another 1–2 *mm* movement from lateral clearance between the pan head and the upper arm. In this study, an extra 4 *mm* is added to the total pan deflection at point **C** due to crosswind.

3.4 Pantograph head displacement calculations

The two (thin surface) collectors of the pan head will be subjected to a lateral crosswind force causing them to deflect. The collectors will also react to a lifting force, which is known to affect the mean variation of the contact force of a pan head [7]. For this work, however, the lift force will not be considered. In the direction of side force, the curved section of each collector is exposed to crosswinds. Each of the curved surfaces may be modelled as a cantilever beam fixed at one end and deflects under an external uniform loading as shown in

Fig. (8). The train's running direction in Fig. (8) is either through or out of the page. The maximum static deflection for each collector is given as [13]

$$y_{\max} = \frac{wl^4}{8EI} \qquad (10)$$

where l is the length of the curved section and w the side load per unit length.

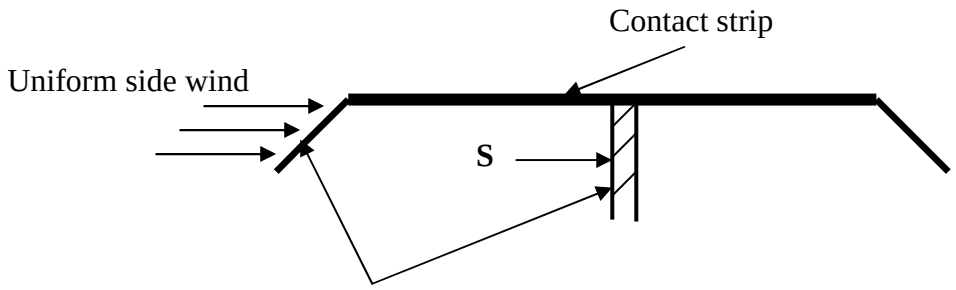

Figure 8: Pantograph head deflection under crosswind

The side force coefficient is that for a flat plate normal to a turbulent flow, i.e. C_D = 1.2 and will react to the instantaneous crosswind. An approximate length of the curved section is about 0.3 *m* and width of approximately 0.03 *m*. Surface **S** in Fig. (8) will also be affected by crosswind but this is not modeled in this work.

3.5 Overhead wire displacement

In this work, only the static deflection of the contact wire under crosswinds for a typical section of the wire between two support masts is considered. Normally, the wire hangs vertically under its own weight with an initial sag in the shape of a catenary. This effect is ignored in the present analysis and the wire is assumed fully stretched horizontally; a situation similar to a wire in cold weather. It is further assumed that the cable is pinned at both ends, has a single span of uniform section, has no attached loads, and will deflect laterally under uniform crosswinds. If the wire is not terminated at each and every end it is possible to consider the problem a continuous beam with multiple supports which is different than a single span. One cannot, however, consider the wire to deflect as a catenary because the wind is not distributed in the same way as the cable's self weight. Copper ($E = 124\times10^9\ N/m^2$) is assumed for the cable. The wire diameter is d_w = 0.0132 *m* and an unstretched length (cable projected length) of L_w = 50 *m*. For simplicity, the "moving force" created due to pantograph/wire contact causing the wire to deflect vertically is not simulated. Due to wire's relatively long length, it can be treated it as a flexible cable. Fig. (9) is an idealisation of the wire deflection under uniform crosswinds. It is also assumed that the supporting pins are at the same elevations, thus for a uniform loading the slope of the cable at mid-span is zero, at which the maximum deflection occurs. The integral length scale of the turbulence at wire height in the lateral direction is of the order of 20 *m* i.e. less than a typical wire span, thus the wire will be assumed to react to mean wind speed U only. Therefore, the side force on the wire is

$$F_{SW} = 0.5\rho A_w U^2 C_{Dw} \qquad (11)$$

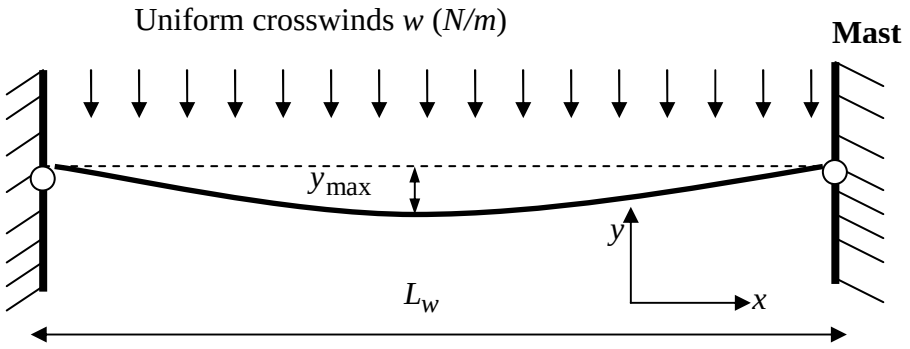

Figure 9: Model of contact wire deflection under uniform crosswinds

Although a typical conductor wire has a cross section profile with wear grooves (in order for it to be gripped by dropper clips and registration arms [15]), such irregularities are ignored so that the area is the complete circular cross sectional area, i.e. $A_w = \pi\left(\frac{d_w}{2}\right)^2$. The unsteady side force F_{SW} acts on the effective area A_{eff} of the cable (a long cylinder) equivalent to that of a rectangular section where its height is the diameter d_w and its length is L_w, so $A_{eff} = d_w \times L_w$. For the side force coefficient, a value of $C_{Dw} \sim 1.0$ [14] is chosen for a long circular cylinder in a turbulent flow with a Re number based on a mean crosswind of 20 *m/s* and a cable length of L_w = 50 *m*. The aim is to compute the history of maximum deflection y_{max} at mid-span and compare it with the permissible maximum lateral deflection of the contact wire in crosswinds. The maximum deflection of the wire is computed without taking into account the stiffening effects of the messenger wire and the droppers. However, as will be shown, wire pretension *T* must be taken into account to avoid unreasonable deflection values. Brecknell Willis advise on a pretension value in the range *T* = 10-15 k*N*. If pretension is neglected, it can be shown that the maximum deflection at mid-span is [13]

$$y_{\max} = L_w\left(\frac{3L_w w}{64EA_w}\right)^{\frac{1}{3}} \qquad (12)$$

With pretension, however, the maximum wire deflection at wire mid-span is

$$y_{\max} = \frac{wL_w^2}{8T} \qquad (13)$$

In the latter case, the governing equation for the deflection *y* at any position *x* along the cable is

$$y = \frac{wx(L_w - x)}{2T} \qquad (14)$$

such that maximum deflection occurs at mid-span ($x = L_w/2$). The governing differential equation with boundary conditions of $y = 0$ at both $x = 0$ and $x = L_w$ is

$$T\left(\frac{d^2x}{dx^2}\right) + w = 0 \qquad (15)$$

3.6 Pantograph sway calculations

Pantograph sway is defined as the maximum lateral movement of the pantograph in relation to the track centre line in reaction to dynamic train displacement. In the presence of crosswinds, pantograph sway will be the sum of two displacements: train body displacement (vehicle sway), and pantograph displacement. The pantograph deflection is due to crosswind, mounting clearances, and pantograph lateral flexibility. The UK's Railway Group Standard RGS for the pantograph sway states that it shall not exceed 190 *mm* when running at maximum vehicle speed and maximum cant deficiency with a maximum wind speed of 35 *m/s* at a height of 4.3 *m* above the rails. Current calculations of pantograph sway will allow reviewing and checking of compliance with established standards when the dynamic analysis software Vampire is used. Selected results for the Class 365 EMU pan sway values will be reported as calculated by Interfleet Technology Ltd, UK under project T689 [16].

4 RESULTS AND DISCUSSION

4.1 Pantograph static deflections

Pantograph deflections were computed for 8 cases of mean crosswind speeds: 5, 10, 15, 20, 25, 30, 35 and 40 *m/s*. From Eq. (10) and (11), increasing the magnitude of the crosswind leads to an increase in the side force, with corresponding increments in the maximum deflections of the pantograph and contact wire. The variation of maximum pan deflection with mean crosswind speed is shown in Fig. (10) for a hinge angle of $\theta = 30^{\circ}$. These deflections include the additional 4 *mm* from pan head clearance as suggested by Brecknell Willis**.** The deflections are negligible reaching just ~ 7.5 *mm* at the highest mean crosswind speed of 40 *m/s*. Fig. (10) also shows the variation of maximum pan deflection with mean crosswind for a number of hinge angles. The deflections increase with θ up to $90°$ but then fall at $\theta = 180°$. It is unsurprising that pantograph crosswind deflections are negligible due to the high rigidity of the arms. The variation of head deflection with crosswind speed is shown in Fig. (11), showing that the deflections are practically negligible.

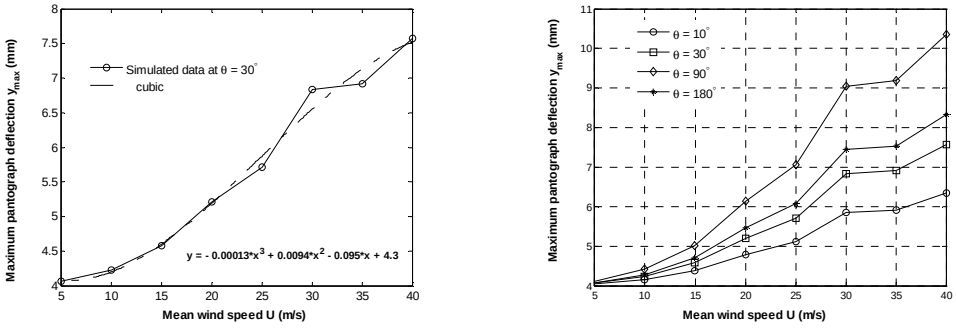

Figure 10: Maximum pan deflection with crosswind; (a) for $\theta = 30°$, (b) for a range of hinge angles

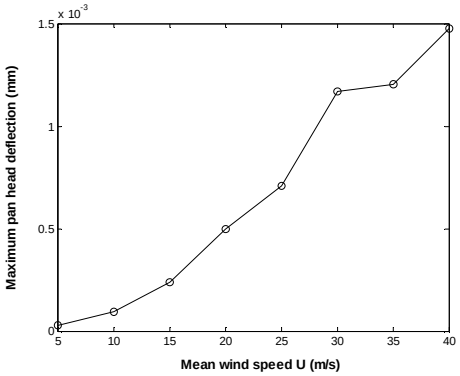

Figure 11: Variation of maximum pan head deflection with crosswind

4.2 Wire deflections

The maximum wire deflection also increases with increasing the crosswind speed as seen in Fig. (12). In order to be able to compare with available data from Network Rail (NR), UK, the wire deflections are computed as a function the three-second gust speed. In terms of mean crosswind, the three-second gust speed may be approximated by the expression

$$U_{gust} = U\left(1 + 2.98\left(\frac{1}{\log(z/z_0)}\right)\right) \qquad (16)$$

Included in Fig. (12) (a) are results for two wire models under crosswinds: one with no wire tension (pinned wire model) and another with wire pretension. Compared to the pantograph, the contact wire movements are quite appreciable (in the range 120 to ~300 *mm*). It is clear that ignoring the wire tension leads to wire deflections under crosswinds being overestimated, nearly as twice as the deflection values with wire pretension. The NR data compares well with the proposed wire model with wire tension, although current results are slightly lower. This gives some confidence that the suggested wire model under crosswinds with pretension is a reasonable one.

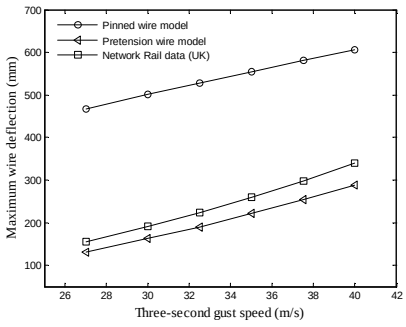

(a)

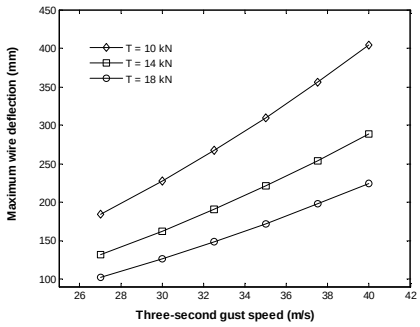

(b)

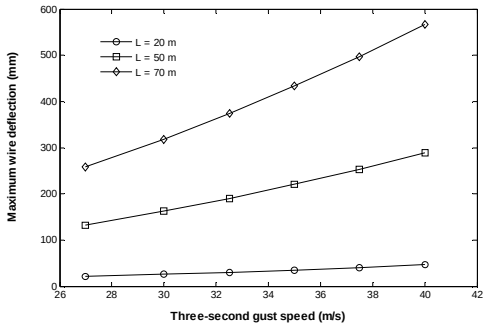

(c)

Figure 12: Wire maximum deflection against gust speed for: (a) different wire models for T = 14 kN and L_w = 50 *m*, (b) different wire lengths, (c) different wire tension

Using the current model with wire pretension and for the wind speeds considered the maximum deflections for three values of tension T = 10, 14, and 18 kN and L_w = 50 *m* are computed as shown in Fig. (12) (b). Increasing the wire tension clearly reduces its tendency to deflect in crosswinds. For the model with wire pretension, Fig. (12) (c) shows the maximum wire deflections in crosswinds for three wire lengths: L_w = 20 *m*, L_w = 50 *m*, and L_w = 70 *m*. It is evident that increasing wire length significantly increases its deflection in crosswinds. The calculations clearly demonstrate that the British Rail requirements on wire deflection under crosswinds are satisfied as set by Network Rail data. Crosswind velocities above 30 *m/s* have been experienced on high embankments and bridges [10], making the issue of wire deflection an important one. The wire length L_w = 50 *m* may, however, represent a higher length than many examples of wire length which could be 20 *m* or 30 *m* long. From a practical point of view, however, using shorter wire lengths is a useful measure to reduce wire deflections but of course it means installing more masts which is a financial burden.

4.3 Overall pantograph wire deflections

The next set of results is for overall pan sway which incorporates the movements of the train body, the pantograph and contact wire.

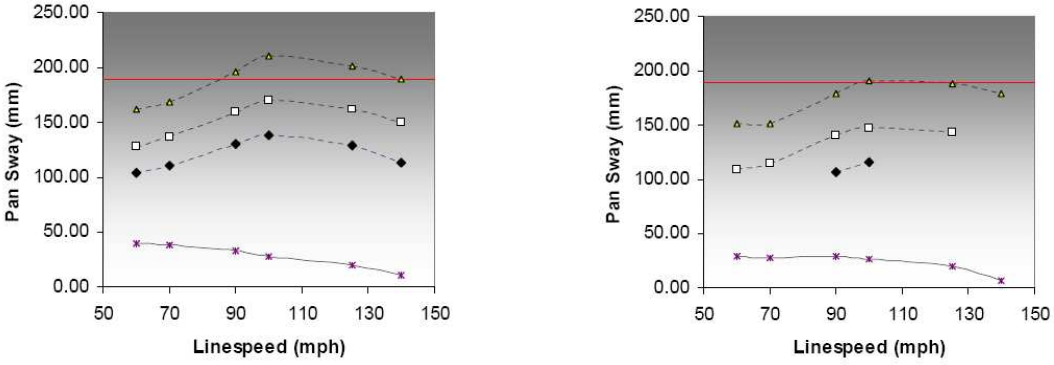

(a) Crush laden condition (b) Tare condition

Figure 13: 96.6 % pantograph sway on a straight track as a function of train and crosswind speeds, at 4.3 *m* pantograph height for the Class 365 EMU [16]

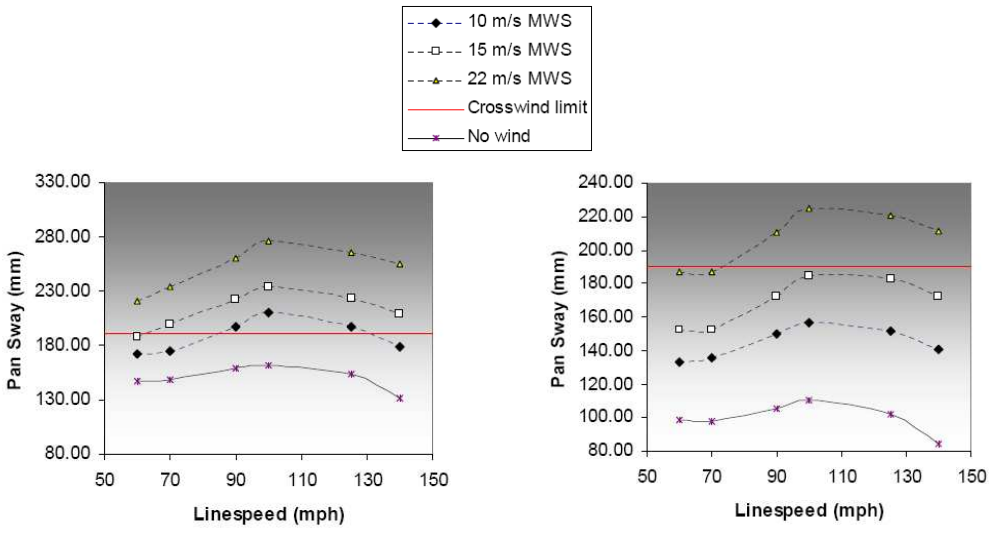

(a) Crush laden condition (b) Tare condition

Figure 14: 96.6 % pantograph sway as a function of train and crosswind speeds, at 4.3 *m* pantograph height and 150 *mm* cant deficiency for the Class 365 EMU [16]

In crush laden and tare conditions, Vampire results for a 4.3 *m* pantograph height are shown when wind blows across a straight track (0 cant deficiency (CD), 0 cant excess (CE)) with track roughness, and when wind is additive to 150 mm CD. Comparisons are made with RGS limits in still air and crosswind for six train speeds (60, 70, 90, 100,125, 140 mph) and three mean wind speeds (10, 15, and 22 *m/s*). Selected results for the 96.6 % pantograph sway are summarised in Fig. 13 and 14. In the crush laden situation with a straight track (see Fig. (13)), the presence of crosswind causes a large increase in the value of pan sway at all train/mean wind speeds, with the case of $U = 22$ *m/s* exceeding the RGS limit beyond 90 mph, reaching a maximum of ~ 215 *mm* at the train's top speed of 100 mph. In the tare condition, however, despite increased pan sway all values were within set limits. When cant deficiency case (CD = 150 *mm*) is simulated at laden condition, the addition of a crosswind increases the pantograph sway well beyond RGS limits, peaking at the train's top speed of 100 mph for all mean wind speeds, then reducing after this speed. For the no wind condition, the pantograph sway is quite insensitive to train speed despite reaching its maximum at 100 mph before starting to decrease.

5 CONCLUSIONS AND FUTURE WORK

Using simplified models of the pantograph of a high speed train and the contact wire, approximate values of their static deflections due to crosswinds have been found. The displacements were then used in Vampire to estimate values of pan sway taking into account train body displacements for different combinations of mean wind and train speeds. When considered individually, the pantograph own displacement in crosswind is only few millimetres while that for the contact wire is much larger, but remains within acceptable limits. Compared with the car body, the pantograph and wire react to different turbulent length scales such that their crosswind deflections do not depend on the train forward velocity. However, the overall pan sway values may exceed RGS limits when the effect of crosswind forces is included, particularly at the train's maximum operating speed. Pan sway variation in still air is quite insensitive to train speed, although it exhibits a similar behaviour in crosswind, peaking at the train's top speed.

For future work, the study could be made more realistic if the dynamic effects are considered rather than the static case alone. This would require dynamic modelling of the pantograph and contact wire using, respectively, mass-spring-damper models and lumped mass models. Given the possible obstruction of aerodynamic uplift on the push-up force of the pantograph it would be interesting to see by how much the pan head will move vertically. For the contact wire model, the initial wire sag due to cable's self weight should be added to the wire's crosswind deflection. The increase in temperature increases the cable's length due to thermal expansion where the change in length may be approximated by $\Delta L_w = L_w \times \alpha \times \Delta T$, where α is the constant of thermal expansion. The impact of different free stream turbulent intensities on the magnitude of crosswind forces and thus the deflections should be studied. The same would be true for various levels of ground roughness. It has so far been assumed that both the wire and pantograph deflect in the same direction whereas in practice they could be deflecting in opposite directions. The aerodynamic side force applied to pantograph is based on 90° crosswind. Consideration should be given to calculating the static deflections at other values of yaw angle, to establish a more complete picture of the pantograph and contact wire performance and hence enable a more robust assessment of dewirement. Due to the presence of springs and dampers around the pantograph elements, certain suspension and structural frequency modes may be excited by wind perturbations of similar frequency. Therefore, this effect should be addressed in dynamic studies.

6 ACKNOWLEDGEMENT

Financial support is greatly received from Railway Safety and Standards Board (RSSB) under contract 1247.

7 REFERENCES

[1] C. J. Baker, M. Sterling, and A. Bouferrouk. Aerodynamic Forces on Electrical Multiple Unit Trains in Cross Winds. Proceedings of the BBAA VI, Milano, Italy, 20-24 July, 2008.

[2] M. Sterling, C. J. Baker, A. Bouferrouk, H. O'Neil, S. Wood, W. Pearce and E. Crosbie. An Investigation of the Aerodynamic Admittances and Aerodynamic Weighting Functions of Trains. Proceedings of the BBAA VI, Milano, Italy, 20–24 July, 2008.

[3] B. Diedrichs, M. Sima, A. Orellano, and H. Tengstrand. Crosswind stability of a high-speed train on a high embankment. Proc. IMechE Vol. **221** Part F: *J. Rail and Rapid Transit*, 205-224, 2007.

[4] E. Andersson, J. Haggstrom, M. Sima, and S. Stichel. Assessment of train-overturning risk due to strong cross-winds. Proc. Instn Mech. Engrs Vol. **218** Part F: *J. Rail and Rapid Transit*, 213-223, 2004.

[5] C. J. Baker. Ground vehicles in high cross winds. Part 2: Unsteady aerodynamic forces. *Journal of Fluids and Structures*, **5**, 91-111, 1991.

[6] M.C. Stickland, T. J. Scanlon, A. Craghead, and J. Fernandez. An investigation into the mechanical damping characteristics of catenary contact wires and their effect on aerodynamic galloping instability. *Journal of Rail and Rapid Transit*, **217**, 63-71, 2003.

[7] A. Balestrino, O. Bruno, A. Landi, and L, Sani. Innovative solutions for overhead catenary-pantograph system: wire actuated control and observed contact force. *Vehicle System Dynamics*, **33**, 69-89, 2000.

[8] J. C. Kaimal, J. C. Wyngaard, Y. Izumi, and O. R. Coté. Spectral characteristics of surface layer turbulence. *Quarterly Journal of the Royal Meteorological Society*. **98**, 563, 1972.

[9] Y. Ding. *The unsteady crosswind effect on trains*, PhD Thesis, The University of Birmingham, 2007.

[10] A. G. Davenport. The Response of Slender Line-like Structures to a Gust Wind. Proceedings of the Institution of Civil Engineers, **23**, 389-408, 1962.

[11] C. J. Baker, A. Bouferrouk, J. Perez, and S.D. Iwnicki. The Integration of Cross Wind Forces into Train Dynamic Calculations. World Congress on Railway Research, Seoul, 18-22 May, 2008.

[12] D.J. Hartland, Developments towards an active pantograph, paper presented at the Institution of Electrical Engineers, London, October 1998.

[13] W. C. Young. *Roark's formulas for stress and strain*. 6th Edition, McGraw-Hill International Editions, 1989.

[14] S. F. Hoerner. *Fluid Dynamic Drag: Practical Information on Aerodynamic Drag and Hydrodynamic*, Hoerner Fluid Dynamics, 1965.

[15] M. A. Gabbott. Catenary and Pantograph Design and Interface. Professional Development Course on Railway Electrification Infrastructure and Systems, 3rd IET, 2007.

[16] H. Oneill. Pantograph Sway and Wire Displacements under Wind Loading, ITLR-T18615-003, Final Report, Interfleet Technology, Derby, UK, 2008.